Experimental and numerical heat transfer from impinging of single free liquid jet

M. A. Teamah [a] and S. Farahat [b]

[a] *Mechanical Eng. Dept., Faculty of Engineering, Alexandria University, Alexandria, Egypt*

[b] *Marine Eng. Technology Dept., College of Maritime Transport and Technology, AASTMT, Alexandria, Egypt*

The heat transfer and fluid flow due to the impingement of vertical circular single jet on a horizontal heated surface is investigated numerically and experimentally. A mathematical model is driven and executed by a computer program, which is prepared for that purpose. The numerical results are presented for range of Reynolds number between 1000 and 40000, showing the variation of both segment and average segment Nusselt numbers as well as the velocity and temperature distribution in the film region. These limits cover the engineering and industrial applications. An experimental apparatus was designed to measure the film thickness distribution, wall temperature and mean temperature of flowing fluid, in order to calculate the segment and average segment Nusselt numbers. Six-volume flow rates were used 1, 2, 4, 5, 6, and 8 liter/minute. A comparison between experimental and numerical results was carried out; it was observed that there is a good agreement between them. From the data obtained either numerically or experimentally it was observed that for all Reynolds number that both segment and average segment Nusselt numbers are reduced with increasing radius ratio especially in the shooting flow region through which they are reduced sharply. Finally the average segment Nusselt number was correlated for two ranges of Reynolds number.

يتناول هذا البحث دراسة انتقال الحرارة والسريان نتيجة تصادم نافورات دائرية مفردة بسطح أفقي ساخن . تمت الدراسة فى هذا البحث بطريقتين الطريقة العددية و الطريقة المعملية التجريبية. بالنسبة للطريقة العددية تمت الدراسة لرقم رينولدز للسريان من١٠٠٠ حتى٥٠٠٠٠, أما بالنسبة للتجارب فقد تم إنشاء جهاز تجريبي لهذا الغرض و الجهاز مزود بدائرة كهربية لقياس سمك طبقة الماء و جهاز لقياس درجة حرارة الماء المتدفق فوق اللوح و درجة حرارة اللوح من خلال مزدوجات حرارية. و تمت الدراسة على ستة قيم لمعدل السريان للنافورة المفردة هم ١و٢و٥و٦و٨ لتر/دقيقة . وثلاث قيم لمعدل السريان للنافورات المتعددة وهي ١و٥و٨ لتر/ دقيقة. المعادلات التفاضلية الخاصة بالسريان و انتقال الحرارة بعد تبسيطها وجد أنها تعتمد على رقم رينولدز.لحساب انتقال الحرارة الموضعي تم مساواة انتقال الحرارة بالحمل من اللوح الساخن بانتقال الحرارة بالتوصيل من خلال طبقات الماء و بعد عمل تكامل لهذه المعادلة أمكن حساب انتقال الحرارة المتوسط. تم عمل برنامج كمبيوتر بلغة الفورتران لحل تلك المعادلات عدديا باستخدام طريقة الحذف لجاوس وبعد ١٢٠٠ محاولة بدأت النتائج تصل لحالة الثبات و كانت أهم هذه الاستنتاجات هي أن انتقال الحرارة يتناسب طرديا مع رقم رينولدز أي معدل السريان وان انتقال لحرارة يقل كلما زاد البعد عن مركز النافورة. تم عمل مقارنة بين النتائج العددية ونتائج التجارب المعملية ووجد توافق بينها. تم استنباط معادلتين رقميتين من النتائج المعملية لحساب رقم نوسلت المتوسط و فى نهاية البحث تم عمل مقارنة بين النتائج الحالية و النتائج السابقة.

Keywords: Heat transfer, Local Nusselt number, Average Nusselt number, Impinging, Free jet

1. Introduction

Impinging of liquid jet on a surface to remove heat from this surface is an effective method for high heat flux heat transfer. Liquid jet on a surface can be widely classified into two configurations, namely submerged and free surface jet. A submerged jet is discharged into stagnant fluid of the same type. On the other hand, a free surface jet is that jet which moves in a medium different from that of the jet. A water jet discharged in air is a free jet while air jet discharged in air is a submerged jet. In recent years, the use of jet impingement as a high performance technique for local heating or cooling a surface has become a well-established method because of its high heat transfer rates and its simplicity in application to a variety of industries. The applications of the impingement technique are

numerous which include drying of paper, textiles, annealing of metals, tempering of glass, cooling of electronic equipment and freezing of tissue in cryosurgery. Due to broad industrial uses of the impinge jets extensive research has been conducted to investigate the hydrodynamic and thermal characteristic of such jets.

2. Literature review

Ven Te Chow [1] studied the phenomena of hydraulic jump and classified the jump according to the value of the Froude number ahead the jump. The cooling or heating of a surface by a jet characterized by the high local heat transfer near the stagnation point and under the shooting flow before the jump. The simplicity of the equipment needed and ease of controlling the process are appreciable features of the heat exchange technique. The mathematical handling of the problem of liquid impingement against surface can be considerably simplified by neglecting the interfacial shear between the film upper free surface and the air in contact with it.

Watson [2] studied analytically both the laminar and turbulent situations of the un-submerged jets. In the shooting regime, the flow filed was divided into two domains. The first is near the stagnation point, where a boundary layer starts to develop on the solid wall in a manner similar to the Balsius layer. The second domain starts at the point where the wall boundary layer reaches the film free surface and ends at the hydraulic jump. Neglecting the gravitational force in the momentum equation.

Riley [3] proposed on an asymptotic expansion to the velocity distribution, ignored the gravitational force and the profile of the free surface to analyze the problem of radial wall jets. Employing Watson velocity distribution inside the film [2], Chaudhury [4] solved the energy equation for heat transfer between the flowing liquid film and an isothermal plate. The viscous dissipation term was retained in the energy equation. Experiments to study the flow and heat transfer of an impinging circular jet on a horizontal plate were performed by Ishigai [5]. The measured film thickness agrees with that calculated by Watson [2] near the center of the jet and deviates as the radial distance increases. Regarding the hydraulic jump as a flow separation induced by the radial gravitational pressure gradient, Kurihara [6] determined the radius of the hydraulic jump. The experimental jump radii measured by Ishigai [5] does not comply with the theoretical ones of Kurihara [6]. Using a laser beam, Craik [7] measured the film thickness and jump radius of a radial jet. Neglecting the presence of a free surface, Inda and Migsaka [8] treated analytically the case of a two dimensional liquid jet impinging on a flat plate heated by a constant heat flux. For a heavy viscous round jet impinging on a plate, J. O. Cruickshank and B. R. Munson [9] arrived to a simple velocity distribution, which approxi-mates the distribution in the free region before the jet.

Zeition [10] studied both analytically and experimentally the flow and heat transfer due to a round water jet falling vertically downwards on an isothermal horizontal plate. Vader et al. [11] measured the local convective heat transfer coefficient between a heated plate and a planner impinging jet. Different jet velocities between 1.8 and 4.5 m/s.

Wang et al. [12] studied analytically the heat transfer between an axisymetric free impinging jet on a solid flat surface with a non-uniform wall temperature or wall heat flux. Both of the exact energy equation and boundary layer energy equation were solved asymptotically. Wall temperature or wall heat flux distribution has considerable effects on the stagnation point. Another analytical investigation was conducted by Wang et al. [13] on the heat transfer in the boundary layer region of a circular free jet impinging on a flat solid surface with non-uniform wall temperature or wall heat flux the flow is laminar incompressible and steady. The solution is matched with that for the stagnation region and the boundary layer region. The results indicate that the Nusselt number for increasing wall temperature or wall heat flux can be considerably higher than that for the constant wall temperature or wall heat flux outside the stagnation region.

Wang et al. [14] investigated analytically the conjugate heat transfer between a laminar free impinging liquid jet and a laterally

insulated disk with arbitrary temperature or heat flux distribution on the surface. The local Nusselt number is found to depend on the Prandtl number of the fluid, the ratio of the fluid to the solid conductivities, the aspect ratio of the solid thickness to the radius of the disk and the prescribed temperature or heat flux distribution. Experiments by Wolf et al. [15] have been conducted on a planner free water jet to investigate the effect of a non uniform velocity profile on the local convection from a plate heated by a constant heat flux. The heat flux varied from 0.24 to 1.47 $M.W/m^2$ and the Reynolds number, based on the average nozzle velocity and nozzle width varied from 15000 to 54000. The flow regime is turbulent. The non-uniform velocity profile has enhanced the heat transfer significantly.

Stevens et al. [16] performed experiments to study the heat transfer between a round jet impinging on a flat plate with a constant heat flux. Effects of the jet Reynolds number, nozzle to plate spacing and jet diameter on heat transfer were investigated. A region of near constant Nusselt number was observed for the region bounded by $0 \le r/d \le 0.75$. The local Nusselt number profile exhibited a sharp drop for $r/d > 0.75$ followed by an inflection and a slower decrease there after. Increasing the nozzle spacing generally decreases the Nusselt number slightly. Correlations for the local and average Nusselt numbers revealed an approximate Nusselt number dependence on the Reynolds number raised to the third power.

Liu et al. [17] studied both analytically and experimentally the heat transfer between a liquid laminar round jet and a plate receiving constant heat flux.

Rahman et al. [18] studied analytically the hydrodynamic and thermal behavior of round and rectangular jets impinging on a horizontal surface. Xin liu, L. A. Galour and J. H. Lienhard [19] study analytically the fluid flow and heat transfer in the stagnation zone of an un-submerged liquid jet. The role of surface tension is emphasized. Stagnation zone transport is strongly dependent on the potential flow above the boundary layer.

Bizzakk et al. [20] studied experimentally the impingement heat transfer coefficient using a laser-induced fluorescence thermal imaging system. Local Nusselt number for four different jets Reynolds numbers, namely, 5800, 8500, 12400 and 17900 have been evaluated. A correlation have been produced for the stagnation point Nusselt number. Measurements were made by C. F. MA and Q. Zheng [21] to investigate the local behavior of the recovery factor and the heat transfer coefficient with free surface circular jets. The experiments were performed with transformer oil jet impinging on a vertical constant heat flux surface from small pipe and orifice nozzles of 1 mm diameter with medium jet velocity about 20 m/sec. H. Sun, C. F. MA and Y. C. Cham [22] studied experimentally the effect of Prandtl number on convection heat transfer due to impingement heat transfer with circular free-surface liquid jets. An empirical formula was developed to correlate all the experimental data. It is noted that the stagnation heat transfer rate slightly decreases with increasing z/d. This trend is consistent with the result reported by Stevens and Webb for water jets [16].

Unsteady heat transfer caused by a confined impinging jet is studied by Yongmann M. Chung and Kai H. Luo [23] using direct numerical simulation. The time-dependent compressible Navier-Stokes equations are solved using high-order numerical schemes together with high-fidelity numerical boundary conditions. A sixth-order compact finite difference scheme is employed for spatial discretization while a third-order explicit Runge-Kutta method is adopted for temporal integration. Extensive spatial and temporal resolution tests have been performed to ensure accurate numerical solutions. The simulations cover several Reynolds numbers and two nozzle-to-plate distances. The correlation between the vortex structures and the unsteady heat transfer is carefully examined. The Nusselt number distribution away from the impingement point, on the other hand, is influenced by the secondary vortices, which arise due to the interaction between the primary vortices and the wall jets.

3. The experimental setup and measuring technique

The general layout of the apparatus is shown in fig. 1. The idea of the apparatus is to

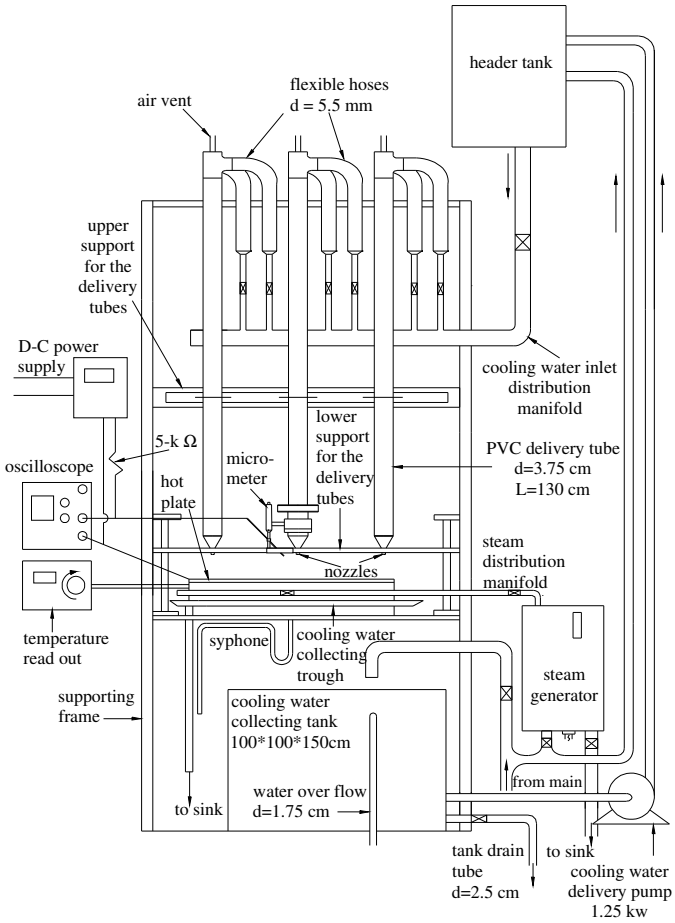

Fig. 1. General lay-out of the apparatus.

let a number of liquid jets directed down wards to flow perpendicular to a fixed horizontal hot plate. This apparatus is designed to be capable of studying experimentally multi-jets. The experiment is implemented with the suitable instruments to control and measure the different variables affecting the phenomena.

3.1. The cooling water circuit

Water is delivered from the main through a control valve to a water storage tank 150cm long, 100 cm wide and 100 cm deep. The tank is provided with outlet tube connected to the suction side of a 1.25 kW water pump. The pump delivers water to a header tank cylindrical in shape, with its base located at a height of 4.5m from the pump level. The header tank is used to provide constant water head to insure constant flow rate of water. The settling of the water in the tank helps in releasing any air or gas bubbles entrapped in the water circuit. This ensures continuous uninterrupted flow through the water circuit. The tank is fed also from the main and it is provided with two sets of water level controlling floats. One for electrically switching on and off the water delivery pump, and the other is connected to the main source. The water is delivered by gravity to a distribution manifold. At each tube inlet, a gate valve is inserted in order to regulate the flow rate through this tube. Water is then fed to nine vertical PVC tubes via flexible hoses. The inside diameter and length of each PVC tube are 3.91 and 130 cm, respectively. At the top of each PVC tube there is an air vent pipe.

On the lower end of each PVC tube a nozzle is screwed for controlling the water out flow from the tube. A third movement is admissible by the mechanism holding the bar. It enables the motion in the vertical direction either upward or downward of the cross bars for controlling the distance between the nozzle and the hot plate. The idea of the mechanism is displayed in fig. 2.

3.2. The hot plate

The hot plate is manufactured from stainless steel sheet 2.5 mm thickness. It is mounted on the top of the heating chamber. The plate is square with 95cm. Each side of the hot plate is provided with 8 right angle cross bars, in such away that one side of the right angled cross bar fixed with bolts in the side of the hot plate while other side has a drilled allowing for bolt to go through. The right angle cross bar is a flange for fixing the hot plate on the top of the heating chamber.

3.3. Heating chamber

It is manufactured from stainless steel sheet in the form of parallelepiped box. The heating chamber has a square base with 90 cm side, 15 cm height and 2 mm wall thickness. This heating chamber is insulated by two layers of thermal insulations, the first layer is asbestos with 12.5 mm thickness and the second is glass wool with 12 mm thickness. The heating chamber is covered by the hot plate. The heating chamber is manufactured so robust to ensure good sealing of the steam on one hand and to withstand its pressure on the other. The heating fluid is steam slightly superheated and is generated by an electrical steam generator.

3.4. Steam generator

A steam generator with an electric heater 18 kW capacity is used to generate the required heating steam. The heater is composed of three-heater elements 6 kW capacity each at 220 V supply. The amount of generated steam can be regulated by changing the inter-connection between the heaters, the capacity of the heater can be 2 kW, 6 kW, 9 kW, 12 kW or 18 kW. It has cylindrical shape and is insulated with two layers of insulation, the first one is asbestos with 1.27 cm thickness, the other one is 3.84 cm thickness and is made from glass wool.

3.5. Measuring the water film thickness over the hot plate

The water film thickness is less than one millimeter before the hydraulic jump. In order to measure the film thickness accurately a micrometer with 0.01 mm sensitivity, fig. 3 is needed to conduct such measurement. The micrometer is carried on a specially designed

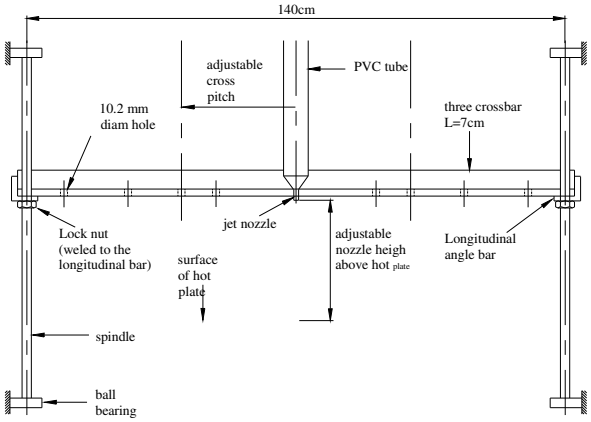

Fig. 2. Mechanism of vertical movement of the jet.

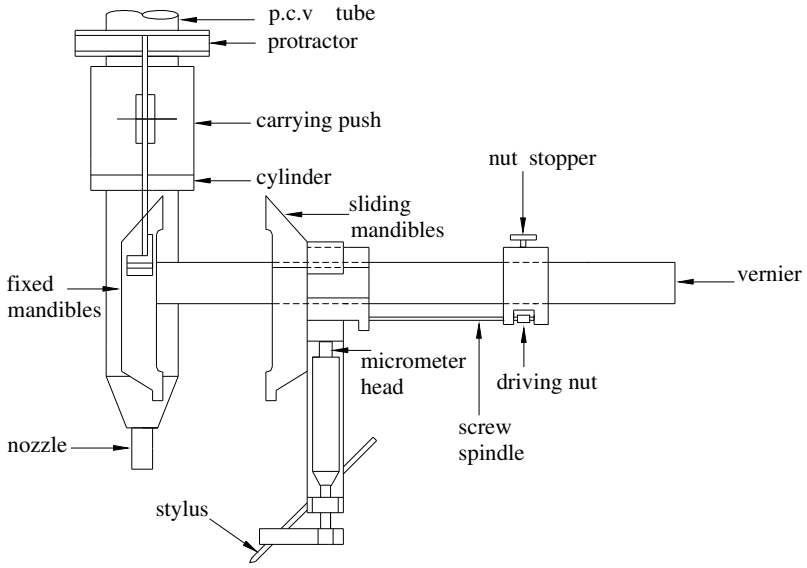

Fig. 3. Mechanism for measuring water film thickness.

mechanism, which can be clamped around any one of the PVC tubes. This mechanism allows the stylus with the micrometer head to rotate concentrically around the respective PVC tube. In order to determine the film thickness, the oscillatory height of the film is first measured and later on an average height can be computed therefore a special electric circuit similar to that described in ref.[10] is used. A D/C power supply manufactured by TRID and capable of producing maximum of 3 Amperes at 25 volt is made to exert 5 volt on a 5 kΩ resistance as shown in fig. 4.

When the stylus tip is in the air above the liquid film, the oscilloscope is supposed to read the voltage of the D/C power supply. If the stylus tip on the micrometer head is advanced till it touches the free surface of the water film, the oscilloscope reading will drop due the reduction in the electric resistance of the parallel circuit of the stylus. If the micrometer head is further proceeded towards the hot plate surface in the water film, the reading gradually decreases until it reaches zero when eventually the stylus contacts the stainless steel plate surface, the full picture of the surface wave over the flowing film can be recorded by the oscilloscope and photo-graphed from its screen. The shape of the wave is integrated to determine the average thickness of the film at this location on the hot plate.

3.6. Measuring the temperature

In the order to determine local Nusselt number of heat transfer between the film and the hot plate at any point, several temperature measurements are needed. A thermocouple with a protective cover of ceramic fixed on micrometer head as shown in fig. 1 is to be used fur measuring temperature gradient through water film beginning from surface of water down to a height of 0.01 mm above the hot plate at least at six points and also measure temperature of cooling water exit from nozzle, this thermocouple can be reconnected to the circuit that was used for measuring fluid film thickness to be used as a stylus. Fig. 4 Oscilloscope circuit for recording the wavy film thickness. Surface temperature of hot plate is measured at 26 points as shown in fig. 5, thermocouples distributed on line OE as follows, starting from center (O) and at distances 5, 20, 35, 50, 65, 80, 95, 110, 130, 140, 160, 180, 200, 220, 240, 260, 280, 300, 320, 340, 360, 380, 400, 420 and 440 mm.

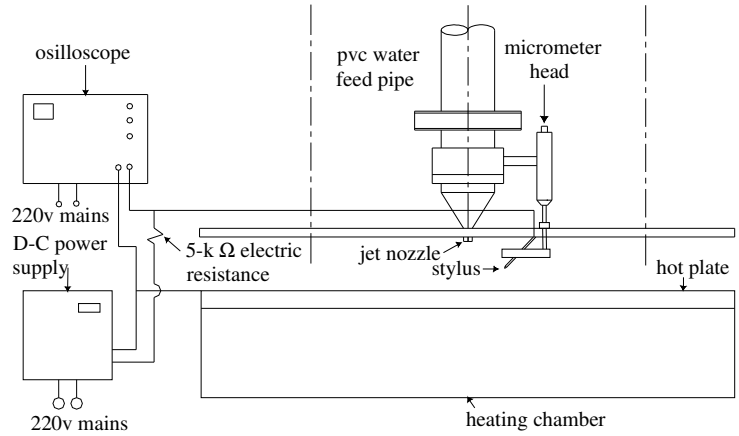

Fig. 4. Oscilloscope circuit.

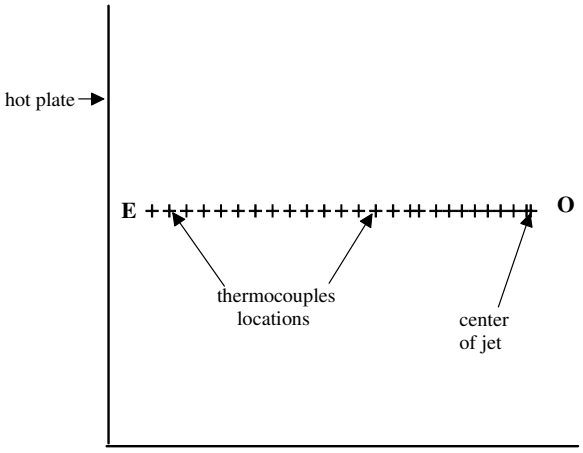

Fig. 5. Locations of thermocouples.

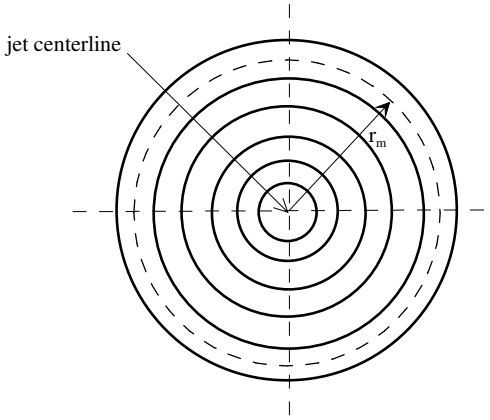

Fig. 6. Circular segments.

4. Data reduction

4.1. Heat transfer coefficient

In order to determine heat transfer coefficient, a heat balance was performed on the mass flowing over the plate. The fluid film thickness is symmetrical around jet centerline; therefore the wall temperature is expected to be also symmetrical. The area around the jet centerline is divided into circular segments each segment has 20 mm width and at constant wall temperature as shown from fig. 6 except the first segment which is a circle with diameter 20 mm, the area of the segment is calculated as follows: $A_n = 0.04\ \pi\ r_m$

4.1.1. Segment heat transfer coefficient

In order to calculate the segment heat transfer coefficient a heat balance for the flowing water is carried out as follows. The thermal energy absorbed by the flowing water over any segment must be equal to the heat transferred from that segment of the plate to the water film, therefore:

$$m\ (Cp_n T_n - Cp_{n-1}\ T_{n-1}) = A_n\ h_n\ (T_{wn} - T_{n-1}).$$

$$h_n = \frac{m(Cp_n T_n - Cp_{n-1} T_{n-1})}{A_n (T_{wn} - T_{n-1})}. \quad (1)$$

4.1.2. Average segment heat transfer coefficient

A heat balance for the flowing liquid is invoked to calculate the average segment transfer coefficient using the principle, thermal energy absorbed by the film must

equal to the heat transferred from the hot plate to the film therefore, for a defined area of the plate, therefore,

$$\bar{h} = \frac{m(Cp_{ex}T_{ex} - Cp_oT_o)}{\sum_1^n A_n(T_{wn} - T_o)}. \quad (2)$$

4.2. Nusselt number

4.2.1. Segment Nusselt number

The segment Nusselt number of plate can be calculated based on segment heat transfer coefficient h_n.

$$Nu_n = \frac{h_n d}{k}. \quad (3)$$

4.2.2. Average segment Nusselt number

The average segment Nusselt number of certain area of the plate can be calculated based on average segment heat transfer coefficient $\bar{h}$.

$$\overline{Nu} = \frac{\bar{h}d}{k}. \quad (4)$$

5. Mathematical model

The differential equations governing the conservation of mass, momentum and thermal energy together with their appropriate boundary conditions are cased. Both fluids used (liquid and air) are considered to be Newtonian constant property. Ax-symmetric jet is used. Therefore, the flow and heat transfer independent variables in the radial and vertical directions will be considered only. Introducing the following dimensionless variables:

$$v_r' = \frac{v_r}{V_j}, \quad v_z' = \frac{v_z}{V_j}, \quad p' = \frac{p}{\rho V_j^2}, \quad z' = \frac{z}{d},$$

$$r' = \frac{r}{d} \text{ and } \theta = (T-T_o)/(T_w-T_o). \quad (5)$$

The two dimensional governing equations are transferred into the dimensionless form by using the above dimensionless groups. The final forms of the governing equations are:

The continuity equation,

$$\frac{\delta v_r'}{\delta r'} + \frac{v_r'}{r'} + \frac{\delta v'_z}{\delta z'} = 0. \quad (6)$$

The momentum equation in radial direction

$$v_r' \frac{\partial v_r'}{\partial r'} + v_z' \frac{\partial v_r'}{\partial z'} = -\frac{\partial p'}{\partial r'} + \frac{1}{Re} \left(\frac{\partial^2 v_r'}{\partial r'^2} + \frac{1}{r'}\frac{\partial v_r'}{\partial r'} + \frac{\partial^2 v_r'}{\partial z'^2}\right). \quad (7)$$

The momentum equation in axial velocity component,

$$v'_r \frac{\partial v'_z}{\partial r'} + v'_z \frac{\partial v'_r}{\partial z'} = -\frac{\partial p'}{\partial z'} + \frac{1}{Re} \left(\frac{\partial^2 v'_z}{\partial r'^2} + \frac{1}{r'}\frac{\partial v'_z}{\partial r'} + \frac{\partial^2 v'_z}{\partial z'^2}\right) - \frac{1}{Fr_j}. \quad (8)$$

The energy equation

$$v_r' \frac{\partial \theta}{\partial r'} + v_z' \frac{\partial \theta}{\partial z'} = \frac{1}{Pr.\,Re}\left[\frac{1}{r'}\frac{\partial}{\partial r'}\left(r'\frac{\partial \theta}{\partial r'} + \frac{\partial^2 \theta}{\partial z'^2}\right)\right]. \quad (9)$$

Applying the dimensionless groups on the different boundary conditions. The boundary conditions are transformed to:

at $r'=0$ symmetrical line

$v_z' = -1$ $v_r' = 0$ and $\frac{\partial \theta}{\partial r'} = 0$,

at $z'=0$ solid boundary, $v_z'=0$, $v_r'=0$ and $\theta = 1$,

at $r' = r_o'$ (out flow),

$$\frac{\partial v_z}{\partial r'} = 0 \text{ and } \frac{\partial v_r}{\partial r'} = 0,$$

and the energy equation applied at out flow, each iteration to correct the calculated dimensionless temperature:

at $z'=L/d$ upper boundary,

if $r'<1/2$, $v'_z = -1$ $v'_r=0$ and $\theta = 0$

if $1/2 < r' < r_o/d$,

$$\frac{\partial v_z'}{\partial z'} = 0, \quad \frac{\partial v_r'}{\partial z'} = 0 \text{ and } \frac{\partial \theta}{\partial z'} = 0.$$

From the above mathematical model, it is clear that the parameters affecting the heat transfer and fluid flow are the jet Reynolds number Re, the fluid Prandtl number Pr, Froude number Fr_j and the ratio between nozzle height and nozzle diameter.

5.1. Film thickness calculations

At each radius, the mass flow in the radial direction for each control volume is calculated. An integration for mass flow is done to reach the mass inlet flow. If the height position of the control volume is less than the film thickness the fluid properties for this control volume is taken the liquid properties. If the control volume lays upper the film thickness the fluid properties is taken as the air properties. The properties for interface control volume is taken by proportional with the mass of each fluid in this control volume.

5. 2. The Nusselt number calculations

The Fourier law states that, the rate of local heat flow by conduction in the fluid layer over the flat plate wall in the radial direction is proportional to the gradient of temperature in that direction,

$$q = -K\frac{\partial T}{\partial z} \quad , \tag{10}$$

where K is the thermal conductivity of the fluid. The local heat flow from the flat plate can also be related to the local heat transfer coefficient between the flat plate and the fluid by:

$$q = h_r\left(T_w - T_\infty\right). \tag{11}$$

Equating eqs. (12), (13) and introducing the dimensionless variables, defined in eqs (8) to (11) we get:

$$Nu_r = -\frac{\partial \theta}{\partial z'}, \tag{12}$$

where Nu_r is the local Nusselt number. The average-local Nusselt number is obtained by integrating the above local Nusselt number:

$$\overline{N}_{uL} = \frac{1}{(r')^2}\int_0^{r'} 2r' Nu_r dr' \, . \tag{13}$$

5.3. The numerical solution

The number of nodes and grid spacing in both the radial and axial directions were examined. The number of nodes used in the solution of the problem was taken as 72 nodes in the radial direction and 82 nodes in the axial direction. The spacing between the nodes in the two directions are uniform. The computer program used for solving the problem is based on the finite volume technique developed by S. Patankar and D.B. [24] which is based on the discretization of the governing equations using the central differencing in space. The iteration method used in this program is a line-by-line procedure, which is a combination of the direct method and the resulting Tri Diagonal Matrix Algorithm (TDMA). Firstly, the accuracy of the solution and the number of iterations were checked.

6. Numerical results and discussion

The selected ranges for Reynolds number is from 1000 to 50000 and for dimensionless radius is from 1 to 50. Practically at Reynolds number less than 1000 there is intermittency in the fluid exit from the nozzle. In-addition, for Re greater than 50000, lots amount of water is consumed and some of water escape away from the flow as sprays. The results include the temperature and radial velocity profiles at different positions, the distribution of both local and average local Nusselt numbers as well as the film thickness distribution.

6.1. Effect of jet reynolds number on local nusselt number.

It is seen from fig. 7 that for all Reynolds numbers the local Nusselt number is very high at dimensionless radius equal 1 and then decreases remarkably with increasing dimensionless radius, this means that the local heat transfer near the stagnation points is very high and decreases with increasing dimensionless radius. For small Reynolds

numbers from 1000 to 10000 and at certain dimensionless radius between 18-35 local Nusselt number begins to increase gradually with increasing dimensionless radius, this can be explained from fig. 8 which contains plot for film thickness with radial velocity and local Nusselt number distributions at different dimensionless radius for Reynolds number equal 2000, The local Nusselt number reaches the minimum value at dimensionless radius 15 and then begins to increase gradually as a result of increasing the fluid velocity. It is also observed from fig. 7 that at Reynolds number ≥ 15000, the value of local Nusselt number decrease at certain dimensionless radius, at this position the temperature difference between wall and fluid at these locations is very small which will be shown later, this reveals that the area of the plate after this radius has not affect on heat transfer process, so it can be said that the optimum area for heat transfer ends at that radius. It is also observed from the same figure. that at dimensionless radius equal 1 the rate of change of local Nusselt number with respect to Reynolds number is very small for Reynolds number equal 10000 and above, so for small area bounded by dimensionless radius equal 1 there is no need to increase Reynolds number more than 10000. Fig. 9 shows dimensionless temperature distribution through film thickness for Reynolds number equal 2000. It is observed that at any dimensionless radius and z/d equal zero the fluid temperature equal the wall temperature, with increasing the dimensionless height the fluid temperature decreases gradually until reaches free stream temperature and at dimensionless radius equal 4 and lower the rate of change of temperature with respect to dimensionless height is considerably higher than that at dimensionless radius higher than 4.

6. 2. Effect of jet reynolds number on the average local nusselt number

It is observed from fig. 10 that for all eynolds number the average local Nusselt number is maximum at dimensionless radius equal one and diminishes remarkably along the radial direction, this means that the heat transfer is high near the stagnation point and decreases with increasing dimensionless radius. It is seen also from the same figure, at

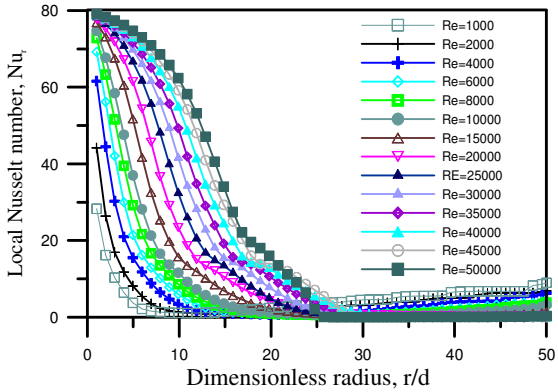

Fig. 7. Effect of Reynolds number on local Nusselt number.

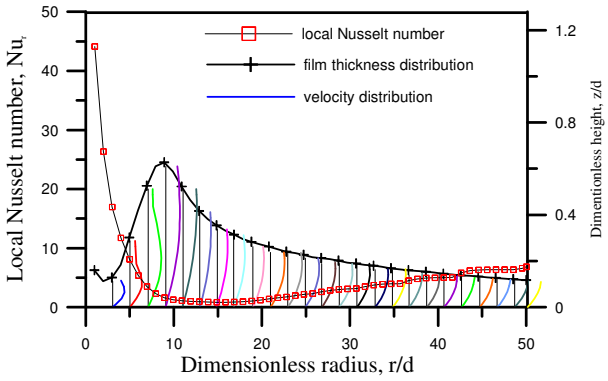

Fig. 8. Dimensionless velocity distribution, local Nusselt number and film thickness at Re=2000.

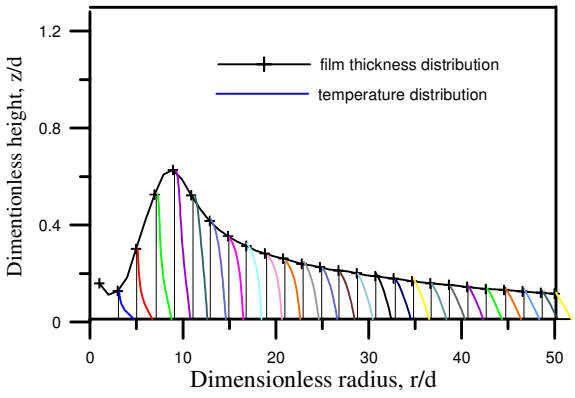

Fig. 9. Dimensionless temperature distribution, local Nusselt number and film thickness, at Re=2000.

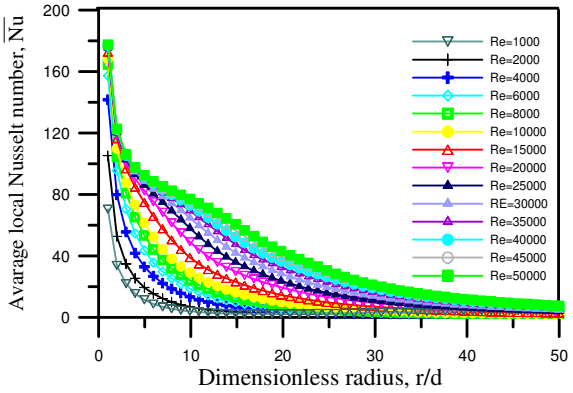

Fig. 10. Effect of Reynolds number on average local Nusselt number.

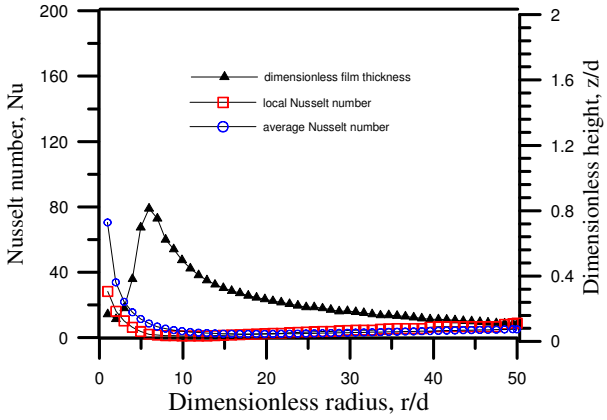

Fig. 11. Local, average local Nusselt number and film thickness for Re=1000.

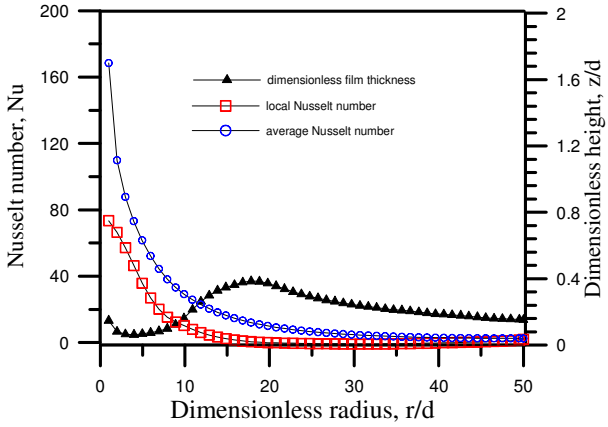

Fig. 12. Local, average local Nusselt number and film thickness for Re=10000.

any dimensionless radius the average local Nusselt number is increased by increasing Reynolds number. The average local Nusselt number is reduced sharply between dimensionless radius1 and 4, this means that there is a sharp reduction also in rate of heat transfer between the same dimensionless radius. At Reynolds number ≥ 15000 and above the rate of change in average local Nusselt number is slightly small, so for small cooling area with radius 4 any increase in Reynolds number more than 15000 has no great effect on the rate of heat transfer.

6.3. Combined effect of reynolds number and dimensionless radius on both local and average, nusselt number and film thickness

It is shown from figs. 11 and 12 that for different Reynolds number and at dimensionless radius equal 1 there is a big difference between local and average local Nusselt number, this confirms that the area bounded by dimensionless radius equal 1 has the largest rate of heat transfer compared with any area larger than that area. It is also shown from the same figures that for all Reynolds number, the average local Nusselt number is very high through the area before hydraulic jump compared with the average local Nusselt number after the hydraulic jump, so the effective area for heat transfer can be consider the area before the hydraulic jump.

7. Experimental results, discussions and comparison

Fig. 13 shows a comparison between the experimental and numerical results for the fluid film thickness distribution with respect to dimensionless radius for flow rates 1, 5 and 8 liter/minute respectivelly. From the figures and the numbers values, the maximum deviation is within 5%, showing a good agreement between the experimental and numerical solution. Fig. 14 shows the effect of Reynolds number on the segment Nusselt number, it is observed that, with increasing Reynolds number the segment Nusselt number is increased, also as the dimensionless radius is increased the segment Nusselt number is increased. It is also seen that the segment Nusselt number is higher in

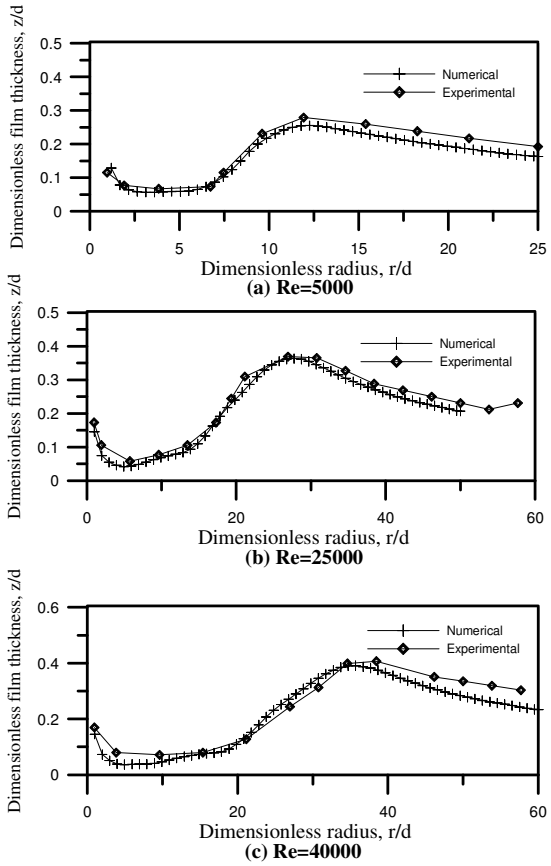

Fig. 13. Comparison between numerical and experimental results for fluid film thickness.

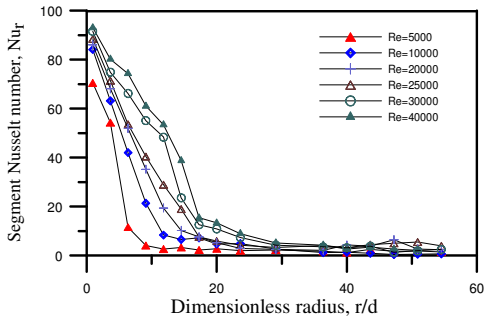

Fig. 14. Effect of Reynolds number on segment Nusselt number.

the shooting flow region as a result of high fluid velocity as concluded from the very low film thickness in this region. This indicates that the results obtained numerically for the fluid velocity showed higher fluid velocity in the shooting flow region than in the streaming flow region. Fig. 15 shows the effect of Reynolds number on the average segment Nusselt number, which shows the same observations as in the numerical results. As the Reynolds number is increased the average segment Nusselt number is increased, also for any Reynolds number the average segment Nusselt number decreased sharply between dimensionless radius 1 and 4. This means that the area of the plate bounded by dimensionless radius 4 has high rate of heat transfer, which agrees well with the numerical results. Figs. 16 through 21 are comparisons between the experimental and numerical results for the variation of segment Nusselt number with respect to the dimensionless radius for Reynolds number 5000, 10000, 20000, 25000, 30000 and 40000 respectively. It is observed that there is a deviation of 14% between the experimental and numerical results for Reynolds number equal 5000 and 18% for Reynolds number equal 40000, this is due to the increased turbulence of fluid exit from the nozzle and the surface roughness. Also deviation between the experimental and numerical results is observed in average segment Nusselt number for the same Reynolds number, as shown from figs. 22 through 27 which indicate the variation of average segment Nusselt number with respect to the dimensionless radius. The minimum deviation equals 3% at Re = 5000 and the maximum equals 15% at Re = 40000. Two correlations (1) and (2) are obtained for average segment Nusselt number for two ranges of Reynolds number with 10% maximum error. The correlations are tabulated in table 1.

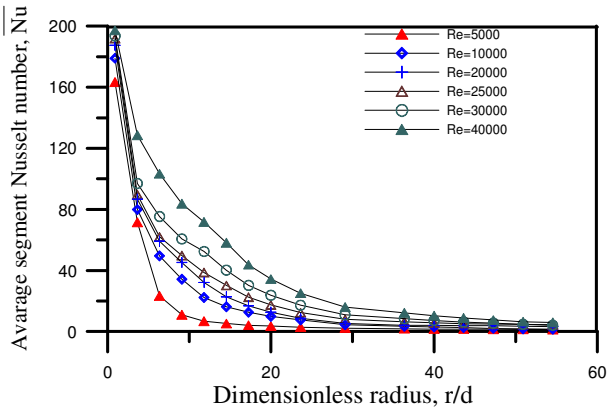

Fig. 15. Effect of Reynolds number on average segment Nusselt number.

Table 1
Correlations for average segment Nusselt number

Re range	r_o/d_j range	Correlation	Error
5000-20000	3.6-54	$\overline{Nu} = 10^{0.755395}(r/d_j)^{-1.50812}\ Re^{0.56188}$	8%
25000-40000	3.6-54	$\overline{Nu} = 10^{-2.25223}(r/d_j)^{-1.15607}\ Re^{1.1528288}$	10%

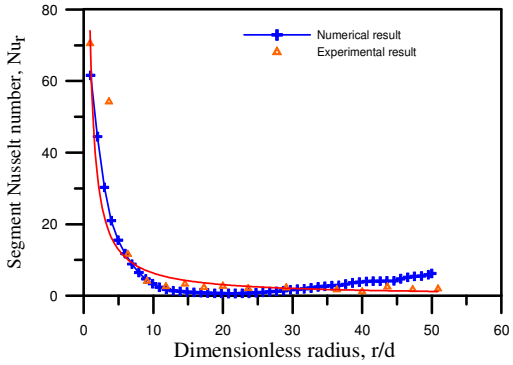

Fig. 16. Comparison between experimental and numerical results of local Nusselt number for Re=5000.

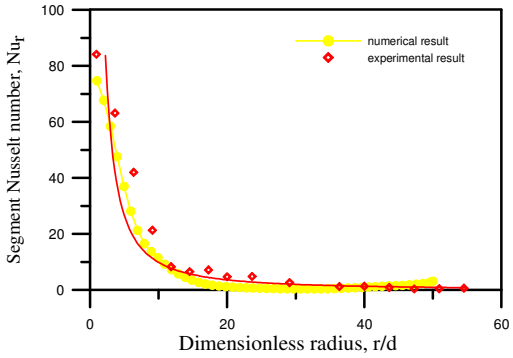

Fig. 17. Comparison between experimental and numerical results of local Nusselt number for Re=10000.

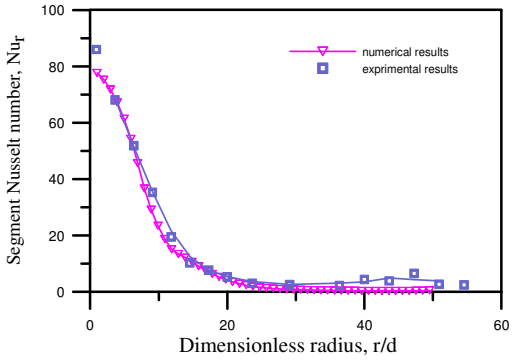

Fig. 18. Comparison between numerical and experimental results of segment Nusselt number for Re=20000.

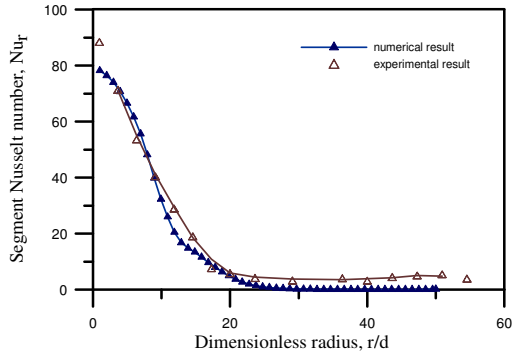

Fig. 19. Comparison between numerical and experimental results of segment Nusselt number for Re=25000.

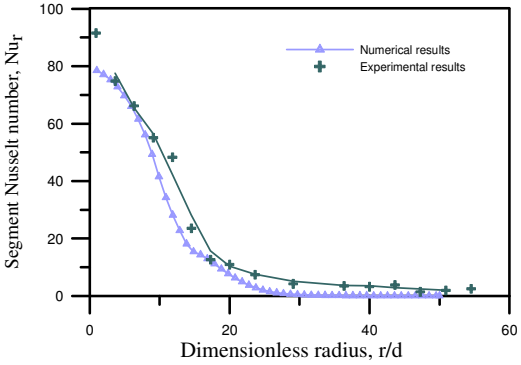

Fig. 20. Comparison between numerical and experimental of segment Nusselt number results for Re=30000.

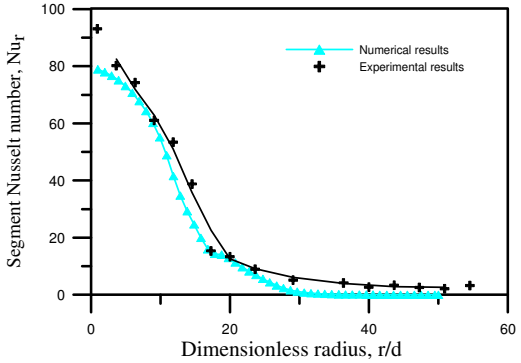

Fig. 21. Comparison between numerical and experimental of segment Nusselt number Re=40000.

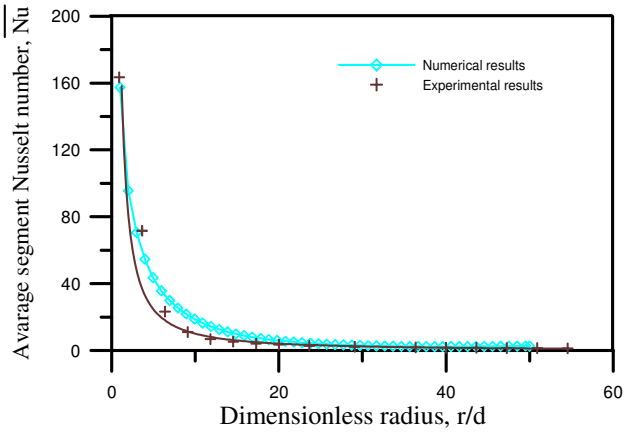

Fig. 22. Comparison between experimental and numerical results of average segment Nusselt number for Re=5000.

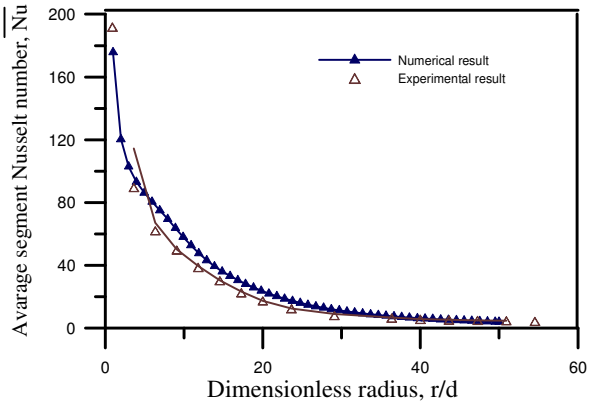

Fig. 25. Comparison between experimental and numerical results of average segment Nusselt number for Re=25000.

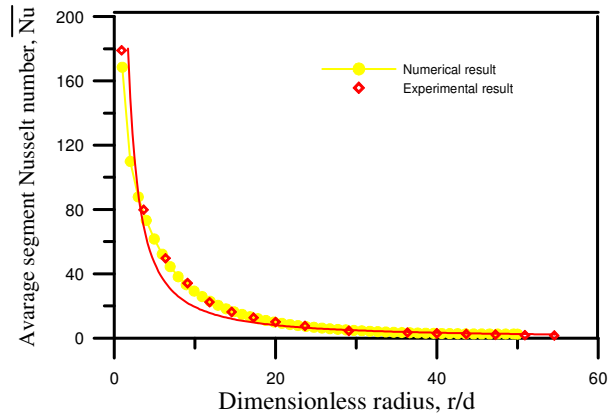

Fig. 23. Comparison between experimental and numerical results of average segment Nusselt number for Re=10000.

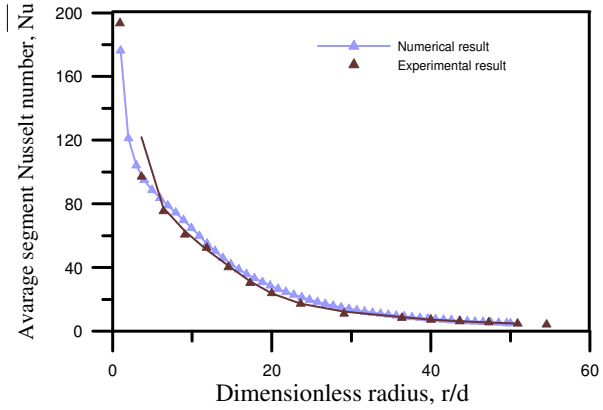

Fig. 26. Comparison between experimental and numerical results of average segment Nusselt number for Re=30000.

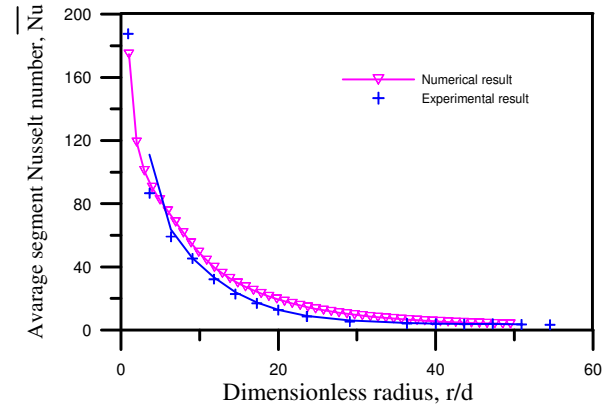

Fig. 24. Comparison between experimental and numerical results of average segment Nusselt number for Re=20000.

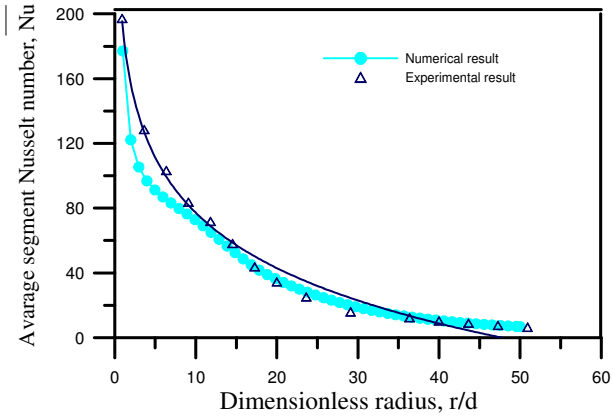

Fig. 27. Comparison between experimental and numerical results of average segment Nusselt number for Re=40000.

8. Comparisons with the previous work

Fig. 28 shows the relation between Reynolds number and average segment Nusselt number at radius ratio 37, the results of Zieton [11] is also plotted on the same figure for the comparison after modification to be compatible with our dimensionless Reynolds number and Nusselt number. It is seen from the figure that Zieton's work is limited to radius ratio 38.46 and Reynolds 17000 but the present result is carried out up to dimensionless radius 50 and Reynolds number 50000, for the range of Zieton results there is a good agreement between the present results and the results of Zeiton specially the experimental results of both. The deviation between the two results come from the retarding effect on the fluid flow due to high range of dimensionless radius for the present results which tend to decrease velocity and so reduction in the average segment Nusselt number, another factor which is that he used only four thermocouples for measuring wall temperature cover 400 mm which is the total diameter of the wall while twenty thermocouples are used for the same diameter in present study which gives better precision. Another comparison with Stevens [16] is carried out for segment Nusselt number versus dimensionless radius as shown in fig 29. for Reynolds number 4000, it shows maximum a deviation of 22% at dimensionless radius equal one. His results is also limited to dimensionless radius equal 8.

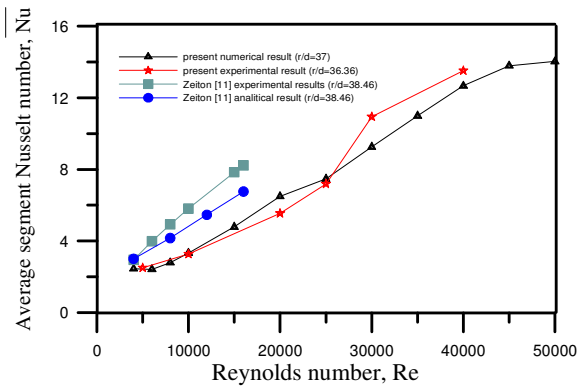

Fig. 28 Comparison with result of Zeiton.

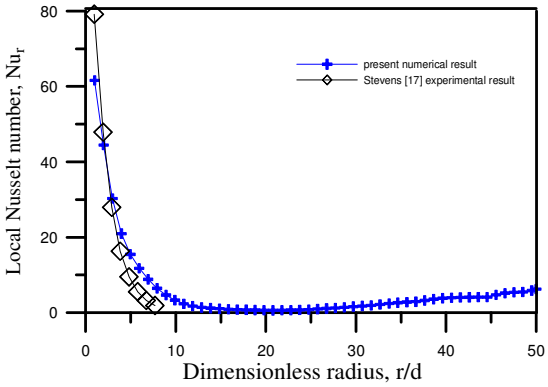

Fig. 29. Comparison between present numerical results and results of Stevens for local Nusselt number at Reynolds number 2000.

9. Conclusions

From the results obtained either numerically or experimentally, it is observed that both segment and average segment Nusselt numbers are higher in the shooting flow region than in the streaming flow region, this is because the fluid film thickness is very small at that region compared with the outer region. This means that the mean velocity of the fluid in that region is higher. It is found also from the comparison of the numerical and experimental results for single jet that there is a good agreement between them. It is seen also that both segment and average segment Nusselt numbers are increased with increasing Reynolds number. For all selected Reynolds numbers, it is clear that the values of average segment Nusselt number sharply decreases between dimensionless radius 1 and 4, this means that the area bounded by small radius ratio has high heat transfer rate. From the numerical results for single jet it is observed that at Reynolds number equal 15000 and above the rate of change in average segment Nusselt number is slightly small. So for small cooling area with dimensionless radius does not exceed 4 any increase in Reynolds number more than 15000 has no significant effect on the rate of heat transfer.

Nomenclature

A_n is the area of segment n, m^2,

Cp Is the specific heat, J/Kg K,

d Is the nozzle diameter, m,

Fr_j is the froude number based on jet velocity, V_j^2/dg,

g Is the gravity acceleration, m/s^2,

$\overline{h}$ is the average segmental heat transfer coefficient, W/m^2 K,

h_r is the segmental heat transfer coefficient, W/m^2 K.

k is the fluid thermal conductivity, W/m K.

$\overline{Nu}$ is the average segment Nusselt number, hd/K,

Nu_r Is the segment Nusselt number, $h_r d/K$,

Pr Is the prandtl number, $\mu Cp/K$,

Q Is the volume flow rate of water, m^3/s,

q Is the heat flux, W/m^2,

r is the radial coordinate, m,

r' is the dimensionless radial coordinate, r/d,

r_j is the radius of hydraulic jump, m,

r_m is the mean radius of circular segment, m,

Re is the reynolds number, $V_j d/\nu$,

T is the fluid temperature, ^oC,

T_o is the jet temperature, ^oC,

T_w is the wall temperature, ^oC,

V_j is the jet velocity, m/s,

v_r is the radial velocity, m/s,

v_r' is the dimensionless radial velocity component, v_r/V_j,

v_z is the axial velocity component, m/ s,

v_z' is the dimensionless axial velocity component, v_z/V_j,

z is the axial coordinate, m,

Z' is the dimensionless axial component, z/d, and

Z is the average water film thickness.

Greek symbols

α is the thermal diffusivity, m^2/s,
ρ is the fluid density, Kg / m^3,
μ is the dynamic fluid viscosity, Kg/m s,
θ is the dimensionless temperature, $(T-T_o)/(T_w-T_o)$,
υ is the kinematic fluid viscosity, m^2/s,
ϕ is the angular coordinate, rad.

References

[1] Ven Te chow, "Open Channel Hydraulics" McGraw-Hill, Japan (1959).

[2] E. J. Watson, "The Radial Spread of a Liquid Jet Over a Horizontal Plane" J. Fluid Mech., Vol. 20, Part3, pp. 481-499 (1964).

[3] N. Riley, "Asymptotic Expansions in Radial Jets" Journal of Mathematics and physics, Vol. XLI (2) (1962).

[4] Z. H. Chaudhury, "Heat Transfer in Radial Liquid jet" J. Fluid Mech, Part3, pp. 501-511 (1964).

[5] S. Ishigai, S. Nakanishi, M. Mizuno, and T. Imaura, "Heat Transfer of the Impinging Round Water Jet In The Interference Zone of Film Flow Along the Wall" JSME, Vol. 20 (139) pp. 85-92 (1977).

[6] M. Kurihara, Report of the Research Institute for fluid Engineering, Kyusyu Imperial University, (3-2) 11. As reported in [8] (1946).

[7] D. D. Craik, R.C. Latham, M. J. Fawkes and P. W .F Gribbon, "The Circular Hydraulic Jump" J. Fluid Mech., Vol. 112, pp. 347-362 (1981).

[8] S. Inada, and Y. Miyasaka, "A Study on the Laminar Flow Heat Transfer between a Two Dimensional Water Jet and a Flat Surface", JSME, Vol. 24 (196) pp. 1803-1810 (1981).

[9] J.O. Cruickshank, and B.R. Munson, "The Viscous-Gravity Jet in Stagnation Flow", ASME Journal of Fluids Engineering, Vol. 104, pp. 360-362 (1982).

[10] O. M. Zeiton, "Convective heat Transfer in the Presence of a Free Surface" M.Sc. Thesis, Dep. Of Mechanical Engineering, Univ. of Alexandria, September (1988).

[11] D. T. Vader, F. P. Incropera, and R. Viskanta, "Local Convective Heat Transfer From a Heated Surface to an Impinging, Planer Jet of Water", Int. J. Heat and Mass Transfer, Vol. 34 (3) pp. 611-623 (1991).

[12] X.S. Wang, Z. Dagan and L.M. Jiji, "Heat Transfer between a Cicular Free Impinging Jet and a Solid Surface, with Non-Uniform Wall Temperature or Wall Heat Flux-1. Solution for the Slagnation Region", Int. J. Heat Mass Trensfer, Vol. 32, pp. 1351-1360 (1989).

[13] X. S. Wang, Z. Dagan and L. M. Jiji, "Heat Transfer between A Circular Free Impinging Jet and a Solid Surface with Non-Uniform Wall Temperature or Wall Heat Flux-2. Solution for the Boundary Layer Region", Int. J. Heat Mass Transfer, Vol. 32, pp. 2189-2197 (1989).

[14] X. S. Wang, Z. Dagan and L.M. Jiji, "Conjugate Heat Transfer between A Laminar Impinging Liquid Jet and a solid Disk", Int. J. heat mass Transfer, Vol. 32, pp. 2189-2197 (1989).

[15] D. H. Wolf, R. Viskanta, and F. P. In Caopera, "Local Convective Heat Transfer from a Heated Surface to a Planer Jet of Warer With a Nonuniform Velocity Profile", ASME Journal of Heat Transfer, Vol. 112, pp. 899-905 (1990).

[16] J. Stevens, and B.W. Webb, "Local Heat Transfer Coefficients Under an Axisymmetric, Single Phase Liquid Jet", ASME Journal of Heat Transfer, Vol. 113, pp. 71-72 (1991).

[17] X. LIU, J. H. Leinhard, and J.S. Lombara, "Convective heat Transfer by impingement of Circular Liquid Jets', ASME Journal of Heat Transfer, Vol. 113, pp. 571-582 (1991).

[18] M. M. Rahman, W. L. Hankey and A. Faghri, "Analysis of the Fluid Flow and Heat Transfer in a Thin Liquid Film in the Presence and Absence of Gravity", Int. J. Heat Mass Transfer, Vol. 34, No.1, pp. 103-114 (1991).

[19] Xin Liu, L.A. Gabour and J. H. Liembard v, "Stagnation-Point heat Transfer During Impiningment of Laminar Liquid Jets; Analysis Including Surface tension", ASME Journal of Heat Transfer, Vol. 115, pp. 99-105 (1993).

[20] D. J. Bizzak and M. K. Chyu, "Use of A Laser Induced Fluorescence Thermal Imaging System for Local Jet Impingement Heat Transfer Measurement", Int. J. Heat Mass Transfer, Vol. 38, pp. 267-274 (1994).

[21] C. F. Ma and Q. Zheng, "Local Heat Fransfer and Recovery Factor with Impinging Free-Surface Circular Jets of Transforms Oil", Int. J. Heat Mass Transfer, Vol. 40, pp.4295-4308 (1997).

[22] H. Sun, C. F. Ma and Y. C. Chen, "Prandtl Number Dependence of Impingement heat transfer with Circular Free Surface Liquid Jets", Int. J. Heat Mass Transfer, Vol. 41, pp. 1360-1362 (1997).

[23] Yongmann M. Chung and hai H. Luo, "Unsteady Heat transfer analysis of an Impinging jet", ASME Journal of Heat Transfer, Vol. 124, pp. 1039-1048 (2002).

[24] S. V Patanker, "Numerical Heat Transfer and Fluid Flow", McGraw-Hill, New York (1980).

Received August 8, 2003
Accepted September 24, 2003